

## PAPER

## Structural configurations and Raman spectra of carbon nanoscrolls

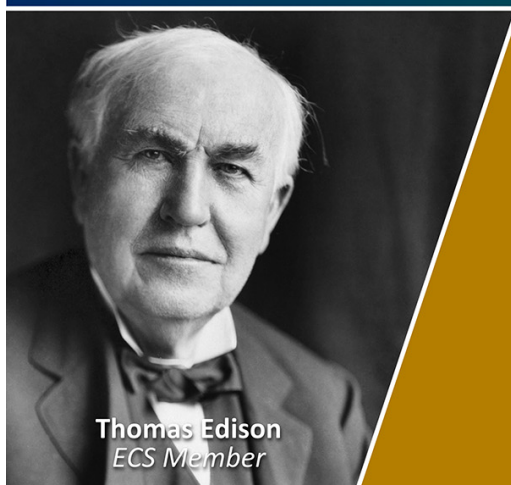
To cite this article: Taewoo Uhm *et al* 2020 *Nanotechnology* **31** 315707

View the [article online](#) for updates and enhancements.

## You may also like

- [Universal production of anisotropic bilayer  \$\text{WSe}\_2\$  nanoscrolls for high-performance photodetector](#)  
Xiang Lan, Fen Zhang, Ziwei Huang *et al.*
- [Controlled fabrication of electrically contacted carbon nanoscrolls](#)  
Marek E Schmidt, Ahmed M M Hammam, Takuya Iwasaki *et al.*
- [Energetics and electronic structure of graphene nanoscrolls](#)  
Yanlin Gao, Mina Maruyama and Susumu Okada

Join the Society  
Led by Scientists,  
for *Scientists Like You!*

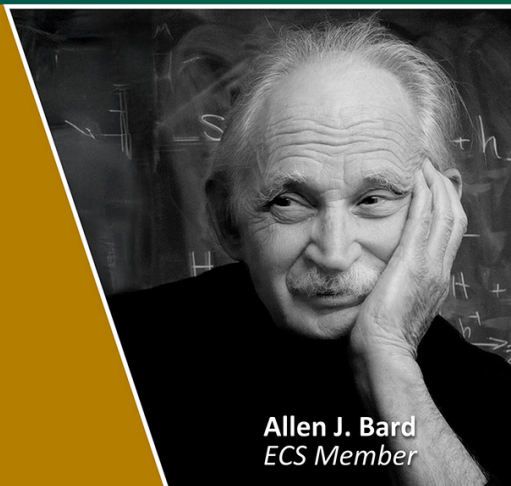


Thomas Edison  
ECS Member



The  
Electrochemical  
Society

Advancing solid state &  
electrochemical science & technology



Allen J. Bard  
ECS Member

# Structural configurations and Raman spectra of carbon nanoscrolls

Taewoo Uhm<sup>1</sup>, Jeonghyeon Na<sup>1</sup>, Jae-Ung Lee<sup>2</sup>, Hyeonsik Cheong<sup>3</sup> , Sang Wook Lee<sup>4</sup> ,  
E E B Campbell<sup>1,5</sup>  and Sung Ho Jhang<sup>1</sup> 

<sup>1</sup> Department of Physics, Konkuk University, Seoul 05029, Republic of Korea

<sup>2</sup> Department of Physics, Ajou University, Suwon 16499, Republic of Korea

<sup>3</sup> Department of Physics, Sogang University, Seoul 04107, Republic of Korea

<sup>4</sup> Department of Physics, Ewha Womans University, Seoul 03760, Republic of Korea

<sup>5</sup> EaStCHEM, School of Chemistry, Edinburgh University, David Brewster Road, Edinburgh EH9 3FJ, United Kingdom

E-mail: [sungho.jhang@gmail.com](mailto:sungho.jhang@gmail.com) and [shjhang@konkuk.ac.kr](mailto:shjhang@konkuk.ac.kr)

Received 12 February 2020, revised 13 March 2020

Accepted for publication 9 April 2020

Published 13 May 2020



## Abstract

Three types of carbon nanoscroll (CNS) structures that are formed when scrolling up graphene sheets are investigated using Raman spectroscopy and atomic force microscopy (AFM). The CNSs were produced from exfoliated monolayer graphene deposited on a Si chip by applying a droplet of isopropyl alcohol (IPA) solution. The three types of CNS are classified as single-elliptical-core, double-elliptical-core (both with large internal volumes) and collapsed ribbon-like, based on AFM surface profile measurements. We discuss the structure and formation of CNS with much larger hollow cores than is commonly assumed and relate this to the large effective 2D bending stiffness of graphene in the IPA solution. The large elliptical core structures show Raman spectra similar to those previously reported for CNS and indicate little interaction between the scrolled layers. The Raman spectra from ribbon-like structures show additional features that are similar to that of folded graphene. These new features can be related to layer breathing modes combined with some resonance enhancement at specific regions of the ribbon-like CNSs that are due to specific twist angles produced when the structure folds/collapses.

Supplementary material for this article is available [online](#)

Keywords: carbon nanoscroll (CNS), scrolled graphene, Raman spectroscopy, atomic force microscopy (AFM), layer breathing mode (LBM), hollow core size

## 1. Introduction

Carbon nanoscrolls (CNSs) are spiral structures composed of a graphene sheet that has been rolled into a scroll. A CNS is structurally similar to a multiwall carbon nanotube (MWNT), however the outermost layer of the CNS is connected to the innermost layer unlike a MWNT which is composed of a few concentric cylindrical nanotubes. Due to this structural characteristic, a CNS has unique properties distinguishable from mono-layer or few-layer graphene and carbon nanotubes (CNT), and can potentially be of interest for a range of applications. Experimental studies have illustrated the potential application of CNS in super capacitors or batteries [1, 2].

Computational studies have suggested many other possibilities e.g. involving the insertion of molecules through the outermost layer edge gap, providing materials suitable for high efficiency hydrogen storage [3, 4] or molecular delivery systems by utilising the tunable hollow core [5, 6] for molecular encapsulation making them more flexible than CNT that have fixed-size, smaller core regions [7–9].

In previous research, measurements of the electrical properties of CNSs showed excellent capacitance values ( $162.2 \text{ F g}^{-1}$  at a current density of  $1.0 \text{ A g}^{-1}$ ) that can be compared with the specific capacity of graphene sheets at  $110 \text{ F g}^{-1}$  [1]. The CNS can sustain a higher current density than MWNT, up to  $5 \times 10^7 \text{ A/cm}^2$  [10], because current flows

through the whole scrolled graphene layer. Raman spectra of CNS typically resemble that of mono-layer graphene rather than multi-layer graphene (MLG), because of the incommensurate layer stacking between the scroll levels rather than the Bernal stacking found in few-layer graphene [10, 11].

In comparison to the large number of computational studies, there have been relatively few experimental studies that focus on the structure of the CNS. Many of the proposed applications of CNS, based on computational studies, assume a 1 nm scale hollow core and ideal circular-cylindrical geometry. Theoretically, Savin *et al* [12] discussed the formation of not only circular scroll structures from graphene but also other forms such as folded or collapsed structures. Although the collapsed ribbon-like structures have been noted previously as a product of graphene scrolling [10, 11] there have been no detailed studies of their structure or spectroscopy.

In this paper we report the surface profiles of different CNS structures using atomic force microscope (AFM) and investigate their properties using Raman spectroscopy. We show that stable, supported CNS can be formed with much larger hollow cores than previously reported. In addition, newly observed Raman signatures from collapsed ribbon-like structures are discussed in detail and compared to twisted multi-layer graphene.

## 2. Experimental methods

Monolayer graphene from natural graphite (NGS Naturgraphit) was mechanically exfoliated using scotch tape and deposited on a silicon substrate with a 300 nm thick layer of SiO<sub>2</sub>. The SiO<sub>2</sub>/Si substrate was first cleaned by washing in acetone, followed by N<sub>2</sub> drying and then repeating with isopropyl alcohol (IPA) and deionized (DI) water. The number of graphene layers was identified by Raman spectroscopy.

The method used to produce CNS from deposited monolayer graphene ribbons closely follows that originally introduced by Xie *et al* [10]. A droplet of IPA solution (IPA:DI water volume ratio of 1:3) was placed on top of the monolayer graphene on the substrate. Once the solution caused the edges to lift, solvent molecules can be intercalated into the space between layer and substrate, further bending the graphene sheets as described in reference [10]. If the scrolling process was not launched, a pure IPA droplet was added to the original IPA solution on the substrate thus further reducing the surface tension (see below) and leading to an enhanced speed of lift-off from the substrate and rolling/folding of the graphene. As originally discussed in reference [10], the speed of rolling depends on the concentration of IPA.

As reported previously, not all graphene monolayers produced CNS. We found that the scrolling to produce quasi-cylindrical structures was more efficient under conditions of high humidity. Scrolls readily formed during the high humidity conditions of the Korean summer (~70% relative humidity) but were much more difficult to produce during the dry laboratory environment typical for the winter months. An experiment was carried out in which the cleaned SiO<sub>2</sub>/Si substrate was exposed to two different humidity levels for one

hour before the graphene was deposited and the scrolling process was initiated with the IPA:water ratio of 1:3. For substrates stored in a relative humidity of 45 – 50% the scrolling success rate was 44% while for substrates stored in a relative humidity of 15% the success rate dropped to 8%. All CNSs discussed in this paper were fabricated in a humid lab atmosphere (~70% relative humidity). When scrolling was speeded up by adding the additional pure IPA droplet to the initial solution, the result was invariably a collapsed, ribbon-like structure.

A confocal Raman measurement system (Witec, alpha 300R) consisting of an ultrahigh-throughput spectrometer (UHTC) with 600 and 1800 grooves/mm grating and a diode laser (532 nm) was used for the measurements. The laser power was kept below 1 mW (focal spot ~1  $\mu\text{m}^2$ ) to avoid heating of the samples. In order to access the deeper low frequency range below 70  $\text{cm}^{-1}$ , reflective volume holographic filters (Ondax and OptiGrate) were used to reject the Rayleigh-scattered light. In this case, three different wavelength lasers were used: the 514.5 nm (2.41 eV) line of a Ar ion laser, the 532 nm (2.33 eV) line of a diode-pumped solid-state (DPSS) laser, and the 632.8 nm (1.96 eV) line of a He-Ne laser. Raman scattering signals were dispersed by a Jobin-Yvon iHR550 spectrometer with a 2400 grooves/mm grating (400 nm blaze) and detected by a liquid-nitrogen-cooled back-illuminated charged-couple-device (CCD) detector.

The 3D images of CNSs and their cross-section profiles in figure 1 were obtained using a AFM (Park Systems, NX-10) in non-contact mode at room temperature. Silicon cantilevers with a typical tip radius of less than 7 nm were used (Park Systems, PPP-NCHR). The AFM tip-sample convolution effect [13] was taken into consideration when determining the widths,  $w$ , of the CNSs (see figure 1(g)).

## 3. Results and discussion

### 3.1. Structural studies of CNSs

Twenty CNSs were investigated by AFM and a variety of structural forms were observed. Three types of CNSs were identified, illustrated by the 3D AFM images of CNS 1, 2 and 3 in figure 1(d) – (f), with cross-section profiles of each in figure 1(g) – (i).

CNS 1 shown in figure 1(d) is distorted from the ideal circular-cylindrical form (figure 1(a)), showing an elliptical-cylindrical structure in the cross-section due to the interaction with the underlying substrate (figure 1(d)). The height and width along the length of CNS 1 are uniform with a height to width ratio of ~0.30. For the CNS 2 structure, the graphene flake appears to have rolled up from two opposite edges forming two neighbouring scrolls of different sizes (figure 1(e)). Neither of these scrolls is ideally circular but, as with CNS 1 they have a flattened elliptical profile. CNS 3 shown in figure 1(c) is the flattest example and is more ribbon-like in structure. The height along CNS 3 is non-uniform and ranges from 5.1 nm to 35.1 nm with an average height to width ratio of ~0.025. Fourteen CNSs among all twenty fabricated CNSs in this study showed collapsed ribbon-like structures, similar to CNS 3. Quasi-cylindrical structures, such as those illustrated by CNS

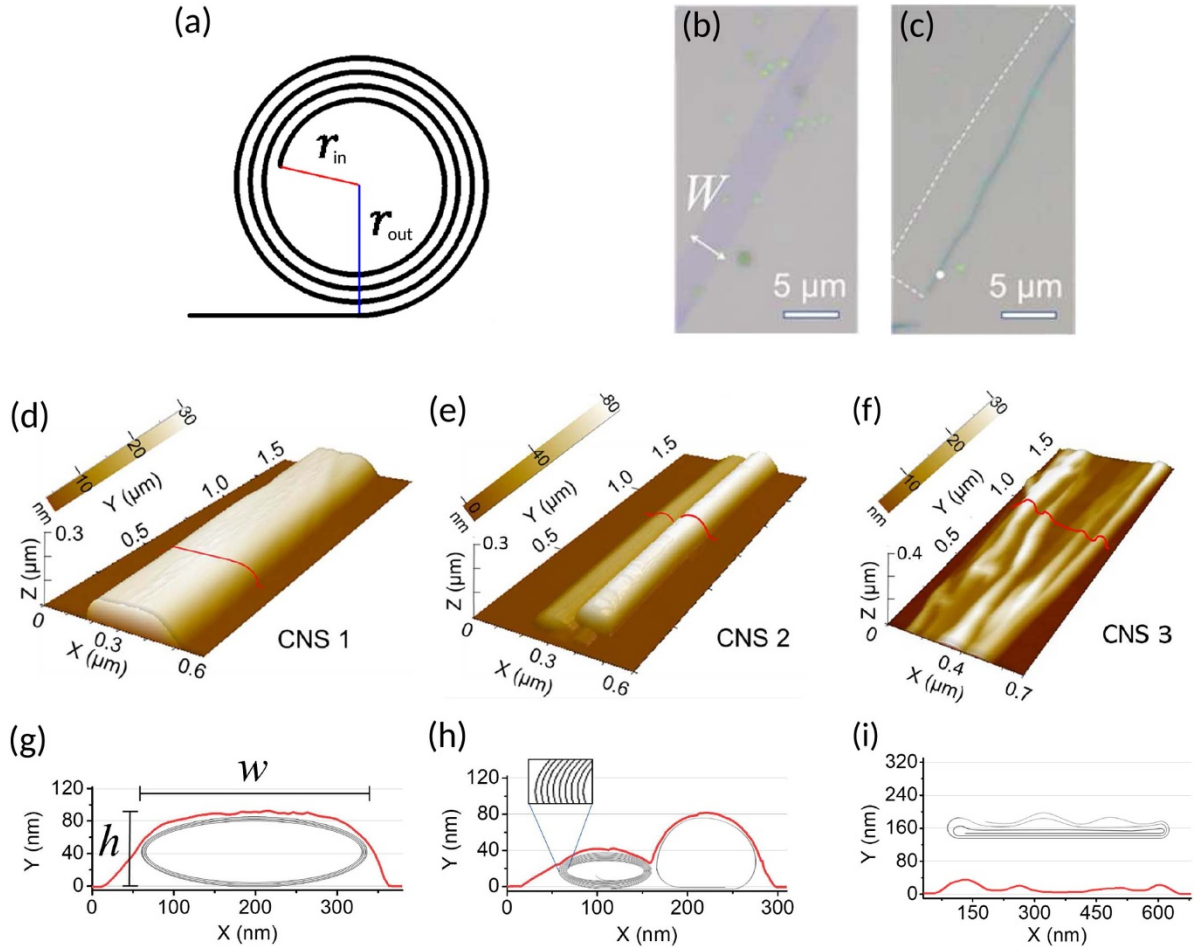


**Figure 1.** (a) Archimedean spiral. The optical images of (b) graphene ribbon, and (c) its scrolled graphene (CNS 2). The white arrow refers to the width of graphene ribbon. The white dashed area in (c) is the shape of graphene before being scrolled. The atomic force microscope (AFM) images of (d) CNS 1, (e) CNS 2 (white spot in (c)) and (f) CNS 3. The profiles of each cross-section (red lines) of (g) CNS 1, (h) CNS 2 and (i) CNS 3. The X, Y scale of them are isotropic.

1 and CNS 2, could be produced when using the 1:3 IPA:water ratio, in which case the graphene rolled slowly over a period ranging from 10 s to 10 minutes. If scrolling was not initiated under these conditions and the additional pure IPA droplet was added to the substrate the graphene rolled up faster than could be followed by eye and the CNS 3 type structure was always produced.

The internal structures can be estimated from a simple calculation. By considering the dimension of the graphene flake prior to scrolling and measuring the cross-section profile of the CNS after scrolling, it is possible to estimate the hollow core size and the number of stacking layers. The scrolls can be considered to have the form of an Archimedean spiral (figure 1(a)). Hence, cylindrical scrolls can be described by the equation in polar coordinates,

$$r_{in} = r_{out} - \frac{d}{2\pi}\theta. \quad (1)$$

Here 0.35 nm [10] is chosen as the interlayer spacing distance  $d$ . Since CNS 1 and CNS 2 are not ideal circular-

cylindrical forms,  $r_{out}$  is modified to account for the elliptical geometry,

$$r_{out} = \sqrt{\frac{(ab)^2}{(b\cos\theta)^2 + (a\sin\theta)^2}}. \quad (2)$$

Here  $a$  and  $b$  are the half width and the half height of the CNS. By knowing the width ( $W$ ) of the monolayer graphene ribbon and the outermost radius  $r_{out}$ , the hollow core radius  $r_{in}$  and the number of stacking layers can be determined. The relation between the width of the graphene sheet  $W$  and  $r_{in}$  is

$$W = \int_{-\pi/2}^{\theta} d\theta' \sqrt{r_{in}^2 + \left(\frac{dr_{in}}{d\theta'}\right)^2}. \quad (3)$$

The lower integration limit is fixed to be  $-\pi/2$  since the graphene rolls up to the opposite edge.

The number of layers and the radii of the hollow cores of CNS 1 and CNS 2 were thus determined by using AFM to measure the width of the monolayer graphene ribbon ( $W$ ) before rolling and the width ( $w = 2a$ ) and height ( $h = 2b$ )



**Table 1.** Structural information for CNS 1, CNS 2 and CNS 3.  $r_{in}$  is the effective hollow core radius of a CNS considering it as a circular scroll.

	$W(\text{nm})$	$w(\text{nm})$	$h(\text{nm})$	$h/w$	$r_{in}(\text{nm})$	rolled turns
CNS 1	2 640	305	90	0.30	105	4.0
CNS 2 (left)	2 000	96	44	0.46	33	9.2
CNS 2 (right)	340	124	81	0.66	48	1.1
CNS 3	8 000	565	5~35	0.01~0.06	177	7.1

of the CNS after rolling (figure 1(g)) taking tip convolution effects into consideration [13]. Assuming that the ribbon-like structures (e.g. CNS 3) were formed from collapsed scrolls, the number of layers of the scroll can be estimated by considering the width of the graphene sheet ( $W$ ) and the cross-sectional profile (figure 1(i)) that was used to estimate the circumference of the outer layer the scroll would have had prior to collapse. This then allows the number of layers and hollow core radius  $r_{in}$  that the structures would have had prior to collapse to be estimated.

The results of the calculations, given in table 1, show that CNS 1 can be estimated to consist of graphene that has been rolled for 4.0 turns, thus composed of 4 stacking layers. By comparing the height of four stacked graphene rolls ( $2 \times 0.35 \text{ nm} \times 4 \text{ layers} = 2.8 \text{ nm}$ ) to the height of CNS 1 (90 nm), it is reasonable to assume that a large hollow core is present in CNS 1 that is estimated to occupy 94% of the volume with an effective hollow core radius, accounting for the elliptical geometry, of  $r_{in} = 105 \text{ nm}$ . Likewise, the heights of both scrolls of CNS 2 are much higher than the heights of the sum of the estimated number of stacking layers, indicating the existence of a large hollow core. However, the height of CNS 3 is much lower and close to the sum of the number of estimated stacking layers (14 layers, giving 4.9 nm). This value is quite close to the minimum height 5.1 nm of the measured cross-section profile of CNS 3, implying that this structure has almost completely collapsed with very little hollow core remaining. The hollow core radii of 17 CNSs are estimated to cover the range from 25 nm to 198 nm (see figure 2). Furthermore, as shown in table 1 and figure 2, the estimated hollow core radii of ribbon-like structures tend to be larger than those of the quasi-cylindrical structures with a critical radius for collapse at around  $r_{in} = 100 \text{ nm}$ .

CNTs are known to deform as the radius of the hollow core increases [14–19], eventually fully collapsing to form a ribbon-like structure or *dog-bone* configuration [14]. The critical radii for collapse range from  $R_{max} = 2.06 \text{ nm}$  for single-wall CNTs (SWNTs) to 2.88 nm for triple-wall CNTs (TWNTs) [18].

The estimated hollow cores for the IPA-fabricated CNSs under study here are much larger. For example, the hollow core of CNS 1 (105 nm) is 37 times bigger than the critical radius for collapse of TWNTs (2.88 nm). Nevertheless, the quasi-cylindrical CNS maintain their hollow core over a time period of at least 6 months under ambient conditions. Previous studies of CNS have reported outer diameters on the order of 10 s of nm with inner cores on the order of a few up to ca. 20 nm

[10] with the largest reported hollow cores to date lying at the lower extreme of our observed structures. It should however be noted that Xie *et al* also reported electrical transport measurements on a CNS with dimensions indicated by an AFM profile to be similar to the quasi-cylindrical structures reported here although the structure of that CNS was not further commented upon [10].

The mechanism leading to scrolling is considered to be the interplay between bending energy and the interlayer binding energy [5]. There have been numerous computational studies of CNS formation and properties [5, 6] based on these considerations. The calculations consistently show stable inner core diameters of a few nm that form the basis for many of the application suggestions for these structures. However, the calculations are usually for isolated graphene sheets and assume a low value for the 2D bending stiffness of the monolayer graphene,  $\kappa$ . Theoretically, this is normally considered to be 1.2 eV based on simulations [20] and measurement of the phonon modes in graphene [21]. Experimental measurements on suspended monolayer membranes in air estimated a higher value of  $7 \pm 3 \text{ eV}$  [22]. Recent experimental studies of the bending rigidity of suspended monolayers in aqueous solution [23] determined effective bending stiffness values approximately three orders of magnitude higher than the value normally assumed for simulations, due to the combination of thermal fluctuations at room temperature and static ripples on the surface of graphene removed from a supporting substrate in solution. Based on these results, Reynolds *et al* discussed the folding of atomically thin membranes in solution in terms of a characteristic length scale for bending,  $L_{EC}$  that is approximately the radius of curvature to which a liquid droplet will bend a rectangular sheet [24, 25]:

$$L_{EC} = \sqrt{\frac{\kappa}{\gamma}}, \quad (4)$$

where  $\gamma$  is the surface tension of the liquid droplet. Using the high effective value of  $\kappa$  for graphene found by Blees *et al* [23],  $10^{-16} \text{ J} \sim 10^{-15} \text{ J}$ , and the surface tension of a 1:3 IPA:water solution ( $\gamma = 28 \text{ mJ/m}^2$  [26]), yields a value for  $L_{EC}$  of approximately 50–200 nm, similar to the typical radii of curvature that we find. We believe that this is the most likely explanation for the large internal radii that we find experimentally. However, there may also be a contribution from the weaker interlayer interaction that may be present in the scrolls due to a slightly larger interlayer spacing compared to bilayer graphene and/or the influence of intercalated water/IPA. The Raman spectra in figure 3 provide some evidence for this. The addition of a pure IPA droplet will reduce the surface tension of the solution [26] and serve two purposes, firstly making it easier to detach the graphene from the substrate and secondly inducing a larger radius of curvature enhancing the likelihood of folding/collapse of the cylindrical structures. The role of humidity can be explained as a means of reducing the interaction energy between the graphene and the  $\text{SiO}_2$ . A single layer of water molecules at the interface will decrease the interaction energy from  $-0.35 \text{ J m}^{-2}$  to  $-0.21 \text{ J m}^{-2}$  [27], enhancing

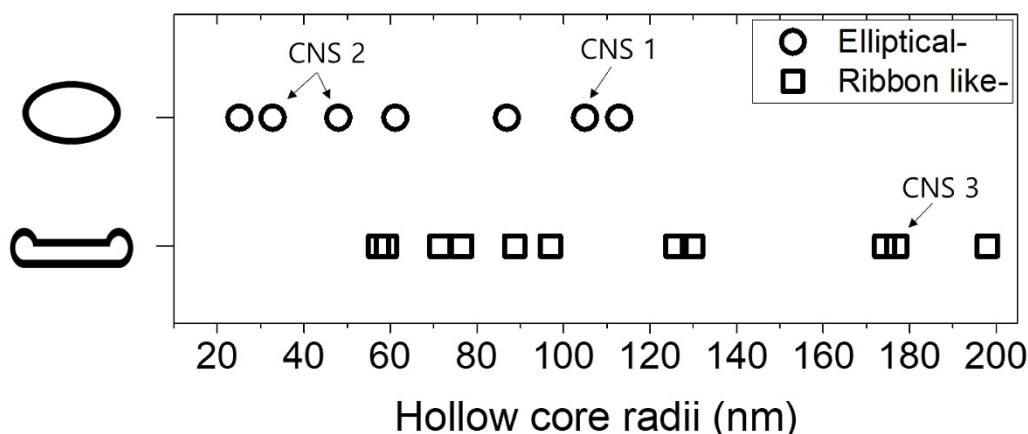


**Figure 2.** The distribution of estimated effective internal radii ( $r_{in}$ ) of elliptical-cylindrical CNS and ribbon-like CNS (prior to collapse).

the probability of lift-off and ease by which the IPA solutions can penetrate under the graphene. The question of how these large cylindrical structures can remain stable over a period of months under ambient conditions still remains unanswered but it is possible that residual water within the structures serves to stabilize them.

### 3.2. Raman spectra of CNS

The Raman spectra were determined for each CNSs using a laser wavelength of 532 nm. Figure 3 compares the Raman spectra of CNS 1, CNS 2 and CNS 3 with that of monolayer graphene. All Raman spectra show very small intensity D peaks ( $\sim 1344 \text{ cm}^{-1}$ ) indicating high-quality graphene with few defects [28], as shown previously for the IPA solution method of producing CNS [10]. All CNS spectra show a blueshift of the 2D mode that can be attributed to the reduction of the Fermi velocity in incommensurately stacked graphene [29]. None of the CNSs in figure 3 show a splitting of the G and 2D peaks, indicating that the degree of curvature induced by scrolling is not sufficient to form distinct G+ and G− peaks [30]. A single 2D peak again shows a small interaction between the layers that is insufficient to cause the splitting of the 2D mode as is observed in AB stacked bi-layer graphene [31]. However, the broadening of the 2D peak compared to ML graphene does show additional evidence for incommensurately stacked graphene layers.

#### 3.2.1. CNS 1 and CNS 2 (elliptical-cylindrical structure).

The Raman spectra from CNS 1 and CNS 2 are very similar and show close similarity to the monolayer graphene spectrum. The ratio of the G to 2D peak intensities is very similar in the cases of CNS 1 and CNS 2 (see table 2). Their ratios values are close to that of Bernal stacked bi-layer graphene and monolayer graphene, but not that of CNS 3 and folded bi-layer graphene ( $t(2+2)\text{LG}$ ) which have G band resonant enhancement. The double-core structure of CNS 2 does not influence its Raman spectrum. The Raman spectra for CNS 1 and CNS 2 are what one would expect for good quality CNS with few defects. The intensities and peak positions remain

the same for different points along the CNS axis. There is no evidence for low frequency modes that can be related to interactions between twisted graphene layers, discussed in detail below for CNS 3. This provides additional supporting evidence for the hollow, cylindrical nature of CNS 1 and CNS 2. If a 2D crystalline sheet is rolled up into a cylinder, the layers formed will be stacked in the same crystalline direction and no twist angle can be introduced unless the structure collapses on itself (see the supplementary video, available online at ([stacks.iop.org/Nano/31/315707/mmedia](https://stacks.iop.org/Nano/31/315707/mmedia))).

**3.2.2. CNS 3 (ribbon-like structure).** The Raman spectrum from CNS 3 in figure 3(a) shows strongly enhanced intensity for both the G and the 2D peaks. This is accompanied by Raman peaks in the low frequency range below  $120 \text{ cm}^{-1}$  and an additional peak at  $1484 \text{ cm}^{-1}$ . From previous research [32, 33], it is known that when graphene is folded or stacked with appropriate twist angles, van Hove singularities in the electronic density of states are induced from the overlap of the two Dirac cones from each layer. The G mode, a doubly-degenerate zone centre ( $\Gamma$ )  $E_{2g}$  phonon mode, is resonantly enhanced due to the resonance between these van Hove singularities and the laser photon energy. Along with the G mode enhancement, a newly-created superlattice wave vector (in a Moire pattern) in the twisted bi-layer graphene causes an R peak to appear within the range  $1460\text{--}1505 \text{ cm}^{-1}$ , depending on the twist angle [34, 35]. Invisible layer breathing modes (LBM) and weak shear modes (C mode), to be found below  $125 \text{ cm}^{-1}$  and  $43 \text{ cm}^{-1}$ , respectively, are seen to co-exist when there is a resonant enhancement of the G and 2D modes [36, 37]. The specific frequencies depend on the number of layers and their relative orientations.

Unlike CNS 1 and CNS 2, the Raman spectrum from CNS 3 is not uniform along the length of the ribbon-like structure. Figure 4 shows Raman map images along the length of CNS 3 corresponding to the G mode (figure 4(b)), the peak that appears at around  $1480 \text{ cm}^{-1}$  (figure 4(c)) and low frequency peaks around  $120 \text{ cm}^{-1}$  (figure 4(d)). The new peaks observed from CNS 3 are clearly correlated with resonance enhancement of the G peak and, in analogy with the

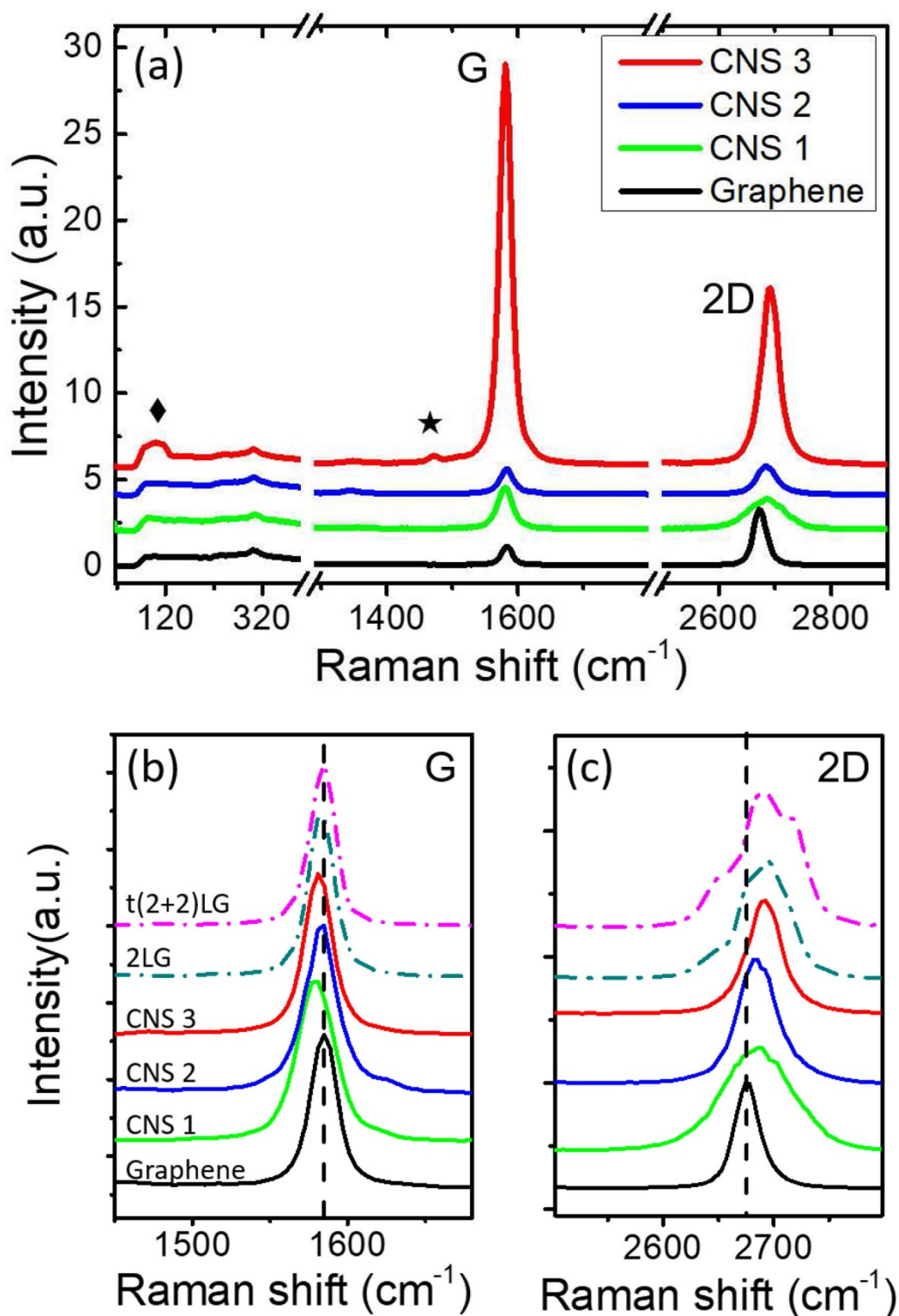


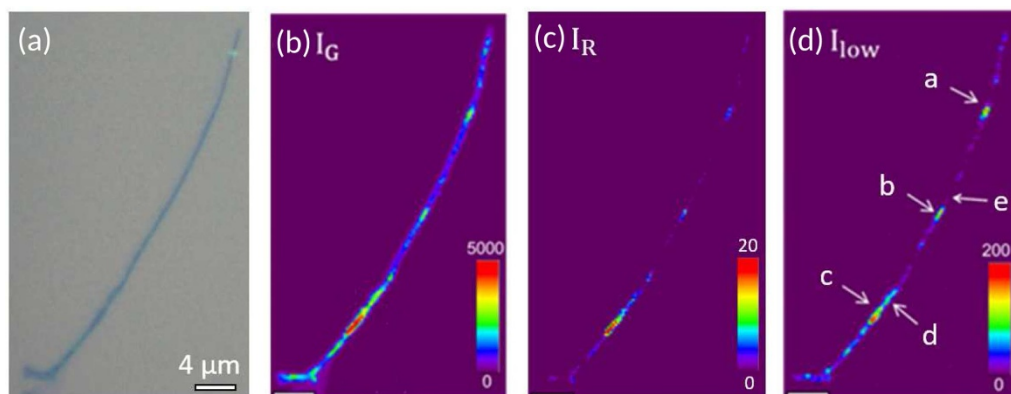
**Figure 3.** (a) The Raman spectra of CNS 1, CNS 2, CNS 3 and graphene for 532 nm laser light (2.33 eV). A low frequency Raman peak appearing around  $119 \text{ cm}^{-1}$  in CNS 3 is marked by  $\blacklozenge$ . The Raman peak appearing around  $1480 \text{ cm}^{-1}$  in CNS 3 is marked by  $\star$ . The tick label is normalized to the height of second-order transverse acoustic mode (2TA) of silicon at  $300 \text{ cm}^{-1}$ . (b) The expanded graph of G peaks in (a). (c) The expanded graph of 2D peaks in (a). All peaks heights in (b) and (c) are normalized to be same to each other. Additional two Raman spectra (dashed dotted line) in (b) and (c) refer to folded and twisted bi-layer graphene (t(2+2)LG) (pink) and Bernal stacked bi-layer graphene (cyan). The black dashed lines in (b) and (c) refer to the position of G and 2D peak of graphene.

studies on twisted bi-layer graphene, can be attributed to R and LBM peaks. It can therefore be assumed that the collapse of large radius cylinders or rapid multiple folding of

the graphene layer as it lifts off from the substrate leads to regions along the ribbon-like structure where slightly different twist angles can be formed in different regions as the upper

**Table 2.** Comparisons of the G mode and 2D mode of graphene, CNSs, Bernal stacked bi-layer graphene (2LG) and folded bi-layer graphene (t(2+2)LG) shown in figure 3. ( $\text{cm}^{-1}$ ).

	Position (G)	FWHM (G)	Position (2D)	FWHM (2D)	I(2D)/I(G)
Graphene	1585	21	2676	27	4.45
CNS 1	1580	29	2685	76	1.73
CNS 2	1583	24	2685	42	2.18
CNS 3	1581	22	2692	37	0.76
2LG	1583	20	2689	—	2.53
t(2 + 2)LG	1584	20	2694	—	0.70

**Figure 4.** (a) Optical image of CNS 3. The Raman mapping images of intensity of (b) G mode, (c) the peaks around  $1480 \text{ cm}^{-1}$  and (d) low frequency region ( $115\text{--}120 \text{ cm}^{-1}$ ) for 532 nm laser light. Several positions are marked as a ~e on CNS 3 in (d), of which Raman spectra are measured and showed in figure 5. The spots a ~d are chosen for where the intensities of low frequency region are strong. The spot e is of no low frequency peaks.

layers collapse onto the lower layers (see the supplementary video).

A comparison of the Raman spectra around the position of the G peak and the low frequency peaks for a series of spots along the CNS 3 structure is shown in figure 5. There are clearly differences in the appearance of the LBM and R peaks at different positions along the structure. This shows that the electronic structure is locally different which could be due to various factors such as locally different strain, curvature, twist angle or stacking configurations induced by the deformation of the scroll structure while collapsing or rapidly folding.

The position of the R peak can be used to estimate the twist angle. Especially, the common range of the peak position observed at spots a ~d, from  $1467 \text{ cm}^{-1}$  to  $1492 \text{ cm}^{-1}$ , corresponds to twist angles within the range  $16^\circ \sim 12^\circ$  [35]. This is in good agreement with the twist angle range that leads to resonant enhancement with 532 nm laser light in twisted multilayer graphene,  $10^\circ \sim 15^\circ$  [33, 35–39]. Note that the spectrum that shows a lower frequency R peak at  $1445 \text{ cm}^{-1}$  (\*), corresponding to a twist angle of  $18^\circ$  also shows a smaller G peak intensity indicating it is not fully resonant (spot e in figure 4). Evidence for the presence of an R' peak is also seen, particularly from the spectra obtained at spots a and e at around  $1620 \text{ cm}^{-1}$  as expected for this range of twist angles [35]. However the contribution of a D' peak ( $\sim 1620 \text{ cm}^{-1}$ ) which is another defect-induced peak cannot be ruled out in this position, particularly for spot a where there is a significant D peak.

The low frequency modes ( $< 130 \text{ cm}^{-1}$ ) show a rich structure that is clearly laser wavelength dependent as shown

in figure 6(a). The low frequency modes are due to relative motions of the graphene planes, either perpendicular (LBM) or parallel (C mode) to their normal [37, 40]. In multilayer graphene, all vibrational modes split due to the confinement in the direction perpendicular to the basal plane and, for a given  $N$ , there are  $N - 1$  C or LB modes, denoted as  $C_{NN-i}$  and  $\text{LBM}_{NN-i}$  ( $i = 1, 2, \dots, N - 1$ ), respectively. Here,  $C_{N1}$  and  $\text{LBM}_{N1}$  (i.e.  $i = N - 1$ ) are the C mode and LBM with the highest frequencies, respectively. A simple relationship has been given for multilayer graphene that relates the LBM frequencies to the number of layers [37]:

$$\text{freq}(\text{LBM}_{NN-i}) = \text{freq}(\text{LBM}_\infty) \sin \left[ \frac{i\pi}{2N} \right], \quad (5)$$

where  $\text{freq}(\text{LBM}_\infty)$  is  $128 \text{ cm}^{-1}$  [37, 41]. Due to selection rules and symmetry constraints, not all modes may be detectable. Spot d for CNS 3 shows the most pronounced peaks in this low frequency range. The influence of resonant excitation is apparent from figure 6(a) where clear peaks are seen for excitation at 514 nm and 532 nm, but this is washed out for 633 nm excitation with the exception of the peak at  $118 \text{ cm}^{-1}$ . No structure in this region is observed for monolayer graphene. Figure 6(b) compares the low frequency range of the 514 nm spectrum from spot c on CNS 3 with the spectrum from folded bi-layer graphene. The folded bi-layer graphene shows a peak corresponding to the highest-frequency breathing mode,  $\text{LBM}_{41}$  at  $116 \text{ cm}^{-1}$  but the other LBMs are not



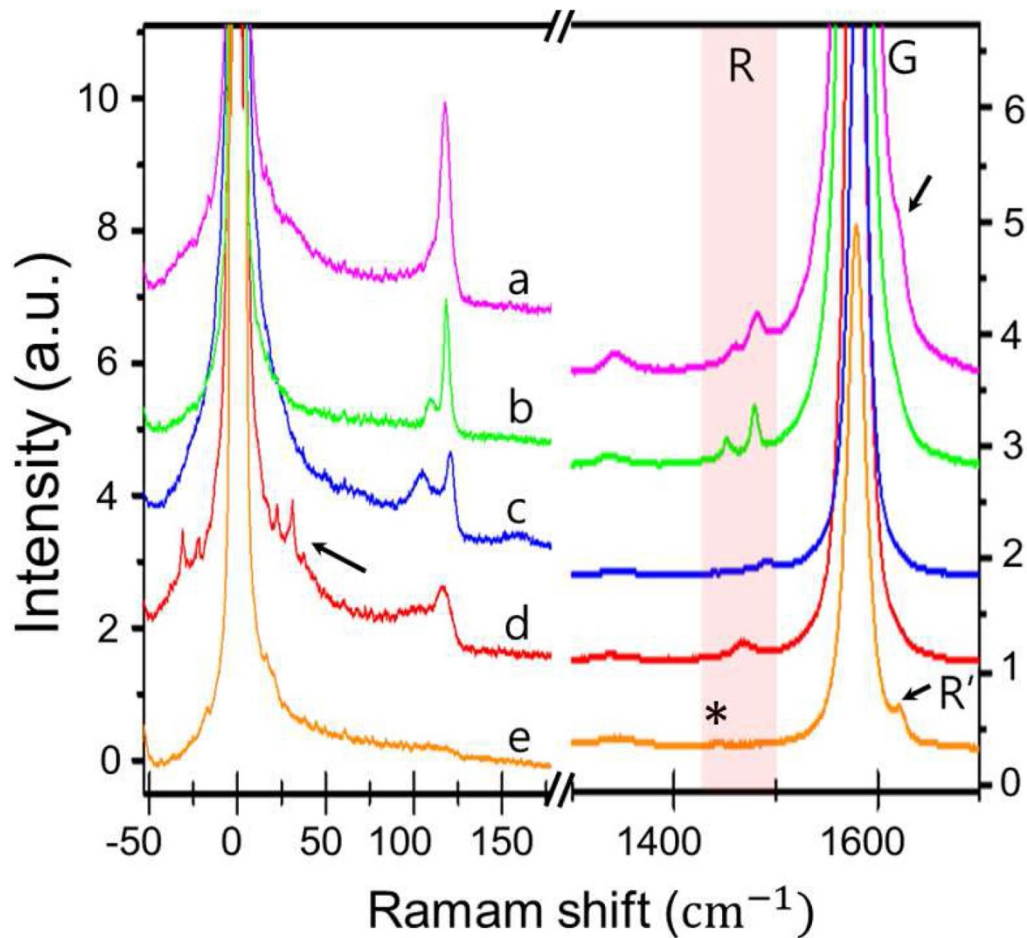


**Figure 5.** The Raman spectra of the spot a~e on CNS 3, which refer to the positions in figure 4(d), for 532 nm laser light. The spots a~d are of strong intensity at low frequency region, and the spot e is of no low frequency peaks. The range from 1430 cm<sup>-1</sup> to 1500 cm<sup>-1</sup> (R peak) is highlighted by red band. Black arrows point to R' peaks at spot a (possibly containing a D' contribution), spot e, and deep-low frequency Raman peaks at spot d. Tick labels are normalized to the height of 2TA of silicon at 300 cm<sup>-1</sup>.

visible in the spectrum. It also shows a relatively strong shear mode C<sub>21</sub>. Shear modes are normally not observed for frequencies > 10 cm<sup>-1</sup> when there is no Bernal stacking component among the stacking layers because any twisted interfaces significantly weaken the shear coupling and push the shear mode frequency towards the Rayleigh line [36, 37]. As shown in figure 6(b), t(2+2)LG shows C<sub>21</sub> at 30 cm<sup>-1</sup>, due to the shear mode between the Bernal stacked bi-layers, not the modes that would be expected for a total of four layers. We therefore do not expect to detect any signals due to C modes in our collapsed nanoscrolls where we do not expect commensurate stacking. The AFM results and modelling discussed earlier estimated that CNS 3 consists of approximately seven rolled turns (table 1) giving a total of approximately fourteen layers for the collapsed structure. The LBM frequencies calculated for  $N = 14$  range from 14 cm<sup>-1</sup> to 127 cm<sup>-1</sup> and have been marked as dashed lines on figure 6(a) and (b) for illustration. It thus appears that the structure observed in the spectrum from CNS 3 can be attributed to the LBMs. It is also remarkable that all modes appear to be present with the strongest intensities for the lowest and highest frequency ranges.

A closer inspection of multiple collapsed ribbon-like structures shows that the highest-frequency LBM (LBM<sub>N1</sub>) observed is red-shifted with respect to the estimated value of approx. 127 cm<sup>-1</sup> for the LBM<sub>141</sub> obtained from equation (5) for the large number of layers present. This is summarized in figure 7. By considering the LBM<sub>N1</sub> observed, it is possible to estimate the interlayer force constant (IFC) for layer breathing coupling between nearest neighbour layers of the CNS,  $\alpha_{\perp}$ . This is done by treating the layers as a linear chain of  $N$  masses connected by springs. The  $\alpha_{\perp}$  is given by [42]

$$\text{freq}(\text{LBM}_{N1}) = \frac{1}{\sqrt{2\pi c}} \sqrt{\frac{\alpha_{\perp}}{\mu}} \sqrt{1 + \cos\left(\frac{\pi}{N}\right)}, \quad (6)$$

where  $\mu = 7.6 \times 10^{-27}$  kg Å<sup>-2</sup> is the graphene mass per unit area, and  $c$  is the speed of light in cm s<sup>-1</sup>. When  $N = \infty$ , the equation is converted into  $\text{freq}(\text{LBM}_{\infty}) = (1/\pi c) \sqrt{\alpha_{\perp}/\mu}$ . Therefore, the IFC of layer breathing coupling of ribbon-like CNSs can be estimated by the measured maximum LBM frequency peak. The IFC is thus  $97 \times 10^{18}$  N m<sup>-3</sup> for the 120 cm<sup>-1</sup> signal in spot c of CNS 3, which is ~12% weaker than that of graphite,  $111 \times 10^{18}$  N m<sup>-3</sup> at 128 cm<sup>-1</sup>.

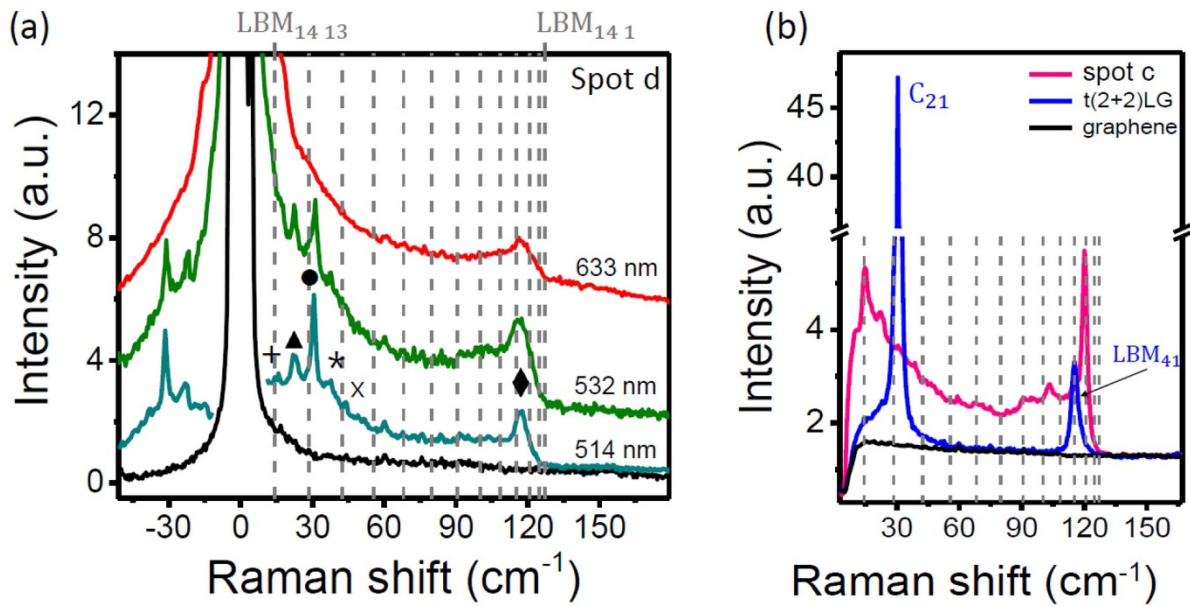


**Figure 6.** (a) The Raman spectra of the spot d on CNS 3 for 514 nm (cyan), 532 nm (green), 633 nm (red) wavelength lasers, and graphene (black) for 532 nm. Several remarkable peaks are marked by +,  $\blacktriangle$ ,  $\bullet$ ,  $\times$  and  $\blacklozenge$ . (b) The comparison of the low frequency Raman spectra of t(2+2)LG (blue), the spot c of CNS 3 (purple), and graphene (black) for 514 nm. Each 13 vertical gray dashed lines in (a) and (b) refer to the calculated LBM frequencies of 14-layers graphite by equation (5) for illustration. The frequencies are from  $14.3\ \text{cm}^{-1}$  to  $127.2\ \text{cm}^{-1}$ , which correspond to  $\text{LBM}_{14\ 13} \sim \text{LBM}_{14\ 1}$ , respectively. Tick labels are normalized to 2TA mode of silicon at  $300\ \text{cm}^{-1}$ .

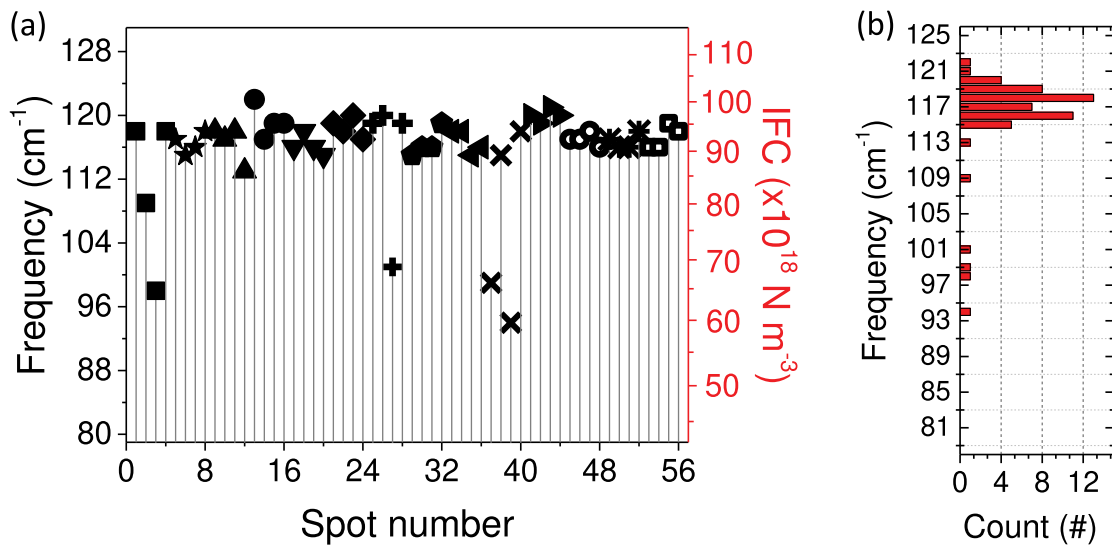


**Figure 7.** (a) The Raman frequency distribution of the highest-frequency LBMs observed at 56 spots in 14 ribbon-like CNSs. The peaks within the same sample are identified by the corresponding symbol. (b) The bar graph of the  $\text{LBM}_{N1}$  shown in (a).

Not only spot c on CNS 3, but most of the highest-frequency peaks of the other ribbon-like CNSs do not reach the bulk graphite value ( $128\ \text{cm}^{-1}$  [37, 41]), the maximum observed was  $122\ \text{cm}^{-1}$  ( $\alpha_{\perp} = 101 \times 10^{18}\ \text{N m}^{-3}$ ) (see figure 7), even though all 14 collapsed CNSs are estimated as having over 10 stacked layers, which is a sufficient number to reach close to the bulk value for the highest frequency mode. It implies that the layers interface coupling of ribbon-like CNSs are weaker than that of Bernal stacking because the inner layers are not firmly stacked, and some residual water layer may be present between the stacked layers.

#### 4. Conclusion

In this paper we have shown the possibility of forming supported, quasi-cylindrical carbon nanoscrolls from monolayer graphene that have much larger inner cores than have usually been assumed. We relate this to the influence of a much higher effective bending stiffness for graphene within the liquid droplet used for scrolling. This provides a significantly larger bending radius for the graphene as it is lifted off the substrate than is commonly simulated. The interplay between bending stiffness, droplet surface tension and humidity thus provides a possibility for tuning the internal core volume of


carbon nanoscrolls over a much larger range than has been previously assumed. We report that nanoscrolls with effective internal radii up to ca. 100 nm are stable under ambient conditions for periods of at least a few months. If the scrolls are formed too quickly and/or the critical bending radius is too large ( $> 100$  nm) the quasi-cylindrical structures collapse to form ribbon-like structures. Detailed Raman spectroscopy studies of these ribbon-like structures show similarities with folded graphene showing new acoustic phonon modes due to layer breathing modes of the collapsed structure. An analysis of the LBM frequencies indicates a slightly weaker interlayer coupling than in multilayer graphene.

## Acknowledgment

This paper was supported by Konkuk University in 2016.

## ORCID iDs

Hyeonsik Cheong  <https://orcid.org/0000-0002-2347-4044>

Sang Wook Lee  <https://orcid.org/0000-0003-2265-4761>

E E B Campbell  <https://orcid.org/0000-0002-4656-3218>

Sung Ho Jhang  <https://orcid.org/0000-0002-8371-5532>

## References

- [1] Zeng F, Kuang Y, Liu G, Liu R, Huang Z, Fua C and Zhou H 2012 Supercapacitors based on high-quality graphene scrolls *Nanoscale* **4** 3997–4001
- [2] Viculis L M, Mack J J and Kaner R B 2003 A chemical route to carbon nanoscrolls *Science* **299** 1361
- [3] Coluci V R, Braga S F, Baughman R H and Galvão D S 2007 Prediction of the hydrogen storage capacity of carbon nanoscrolls *Phys. Rev. B* **75** 125404
- [4] Mpourmpakis G, Tylisanakis E and Froudakis G E 2007 Carbon nanoscrolls: a promising material for hydrogen storage *Nano Lett.* **7** 1893–7
- [5] Shi X, Pugno N M and Gao H 2010 Tunable Core Size of Carbon Nanoscrolls *J. Comput. Theor. Nanosci.* **7** 1–5
- [6] Liu Z, Gao J, Zhang G, Cheng Y and Zhang Y W 2017 From two-dimensional nano-sheets to rollup structures: expanding the family of nanoscroll *Nanotechnology* **28** 385704
- [7] Gao H, Kong Y, Cui D and Ozkan C S 2003 Spontaneous insertion of DNA oligonucleotides into carbon nanotubes *Nano Lett.* **3** 471–3
- [8] Hummer G, Rasalah J C and Noworyta J P 2001 Water conduction through the hydrophobic channel of a carbon nanotube *Nature (London)* **414** 188–90
- [9] Zhao K W and Wu H Y 2015 Fast water thermo-pumping flow across nanotube membranes for desalination *Nano Lett.* **15** 3664–8
- [10] Xie X, Ju L, Feng X, Sun Y, Zhou R, Liu K, Fan S, Li Q and Jiang K 2009 Controlled fabrication of high-quality carbon nanoscrolls from monolayer graphene *Nano Lett.* **9** 2565–70
- [11] Zhou H, Qiu C, Yang H, Yu F, Chen M, Hu L, Guo Y and Sun L 2011 Raman spectra and temperature-dependent Raman scattering of carbon nanoscrolls *Chem. Phys. Lett.* **501** 475–9
- [12] Savin A V, Korznikova E A and Dmitriev S V 2015 Scroll configurations of carbon nonoribbons *Phys. Rev. B* **92** 035412
- [13] Shen J, Zhang D, Zhang F H and Gan Y 2017 AFM tip-sample convolution effects for cylinder protrusions *Appl. Surf. Sci.* **422** 482–91
- [14] Pugno N M 2010 The Design of Self-Collapsed Super-Strong Nanotube Bundles *J. Mech. Phys. Solids* **58** 1397–410
- [15] Elliott J A, Sandier J K W, Windle A H, Young R J and Shaffer M S P 2004 Collapse of single-wall carbon nanotubes is diameter dependent *Phys. Rev. Lett.* **92** 095501
- [16] Tang T, Jagota A, Hui C Y and Glassmaker N J 2005 Collapse of single-walled carbon nanotubes *J. Appl. Phys.* **97** 074310
- [17] Liu B, Yu M F and Huang Y 2004 Role of lattice registry in the full collapse and twist formation of carbon nanotubes *Phys. Rev. B* **70** 161402
- [18] Xiao J, Liu B, Huang Y, Zuo J, Hwang K C and Yu M F 2007 Collapse and stability of single- and multi-wall carbon nanotubes *Nanotechnology* **18** 359703
- [19] Liu J 2012 Explicit Solutions for a SWCNT Collapse *Arch. Appl. Mech.* **82** 767–76
- [20] Fasolino A, Los J H and Katsnelson M I 2007 Intrinsic ripples in graphene *Nature* **6** 858–61
- [21] Nicklow R, Wakabayashi N and Smith H G 1972 Lattice dynamics of pyrolytic graphite *Phys. Rev. B* **5** 4951–62
- [22] Lindahl N, Midtvedt D, Svensson J, Nerushev O A, Lindvall N, Isacson A and Campbell E E B 2012 Determination of the bending rigidity of graphene via electrostatic actuation of buckled membranes *Nano Lett.* **12** 3526–31
- [23] Bles M K et al 2015 Graphene kirigami *Nature* **524** 204–7
- [24] Reynolds M F et al 2019 Capillary origami with atomically thin membranes *Nano Lett.* **19** 6221–6
- [25] Py C, Reverdy P, Doppler L, Bico J, Roman B and Baroud C N 2007 Capillary origami: spontaneous wrapping of a droplet with an elastic sheet *Phys. Rev. Lett.* **98** 156103
- [26] Park J G, Lee S H, Ryu J S, Hong Y K, Kim T G and Busniaina A A 2006 Interfacial and electrokinetic characterisation of IPA solutions related to semiconductor wafer cleaning and drying *J. Electrochem. Soc.* **153** G811
- [27] Gao W, Xiao P, Henkelman G, Liechti K M and Huang R 2014 Interfacial adhesion between graphene and silicon dioxide by density functional theory with van der Waals corrections *J. Phys. D: Appl. Phys.* **47** 255301
- [28] Ferrari A C et al 2006 Raman spectrum of graphene and graphene layers *Phys. Rev. B* **77** 187401
- [29] Ni Z, Wang Y, Yu T, You T and Shen Z 2008 Reduction of Fermi velocity in folded graphene observed by resonance Raman spectroscopy *Phys. Rev. B* **77** 235403
- [30] Dresselhaus M S, Dresselhaus G, Jorio A, Filho A G S and Saito R 2002 Raman spectroscopy on isolated single wall carbon nanotubes *Carbon* **40** 2043–61
- [31] Latil S, Meunier V and Henrard L 2007 Massless fermions in multilayer graphitic systems with misoriented layers: Ab initio calculations and experimental fingerprints *Phys. Rev. B* **76** 201402
- [32] Havener R W, Zhuang H, Brown L, Hennig R G and Park J 2012 Angle-resolved Raman imaging of interlayer rotations and interactions in twisted bilayer graphene *Nano Lett.* **12** 3162–7
- [33] Kim K et al 2012 Raman spectroscopy study of rotated double-layer graphene: misorientation-angle dependence of electronic structure *Phys. Rev. Lett.* **108** 246103
- [34] Carozo V, Almeida C M, Ferreira E H M, Cançado L G, Achete C A and Jorio A 2011 Raman signature of graphene superlattices *Nano Lett.* **11** 4527–34
- [35] Carozo V et al 2013 Resonance effects on the Raman spectra of graphene superlattices *Phys. Rev. B* **88** 085401
- [36] Wu J B, Zhang X, Ijäs M, Han W P, Qiao X F, Li X L, Jiang D S, Ferrari A C and Tan P H 2014 Resonant Raman spectroscopy of twisted multilayer graphene *Nat. Commun.* **5** 5309

- [37] Wu J B *et al* 2015 Interface coupling in twisted multilayer graphene by resonant Raman spectroscopy of layer breathing modes *ACS Nano* **9** 7440
- [38] Wang Y *et al* 2013 Resonance Raman spectroscopy of G-line and folded phonons in twisted bilayer graphene with large rotation angles *Appl. Phys. Lett.* **103** 123101
- [39] He R *et al* 2013 Observation of low energy Raman modes in twisted bilayer graphene *Nano Lett.* **13** 3594–601
- [40] Lui C H, Ye Z, Keiser C, Xiao X and He R 2014 Temperature-activated layer-breathing vibrations in few-layer graphene *Nano Lett.* **14** 4615–21
- [41] Dolling G and Brockhouse B N 1962 Lattice vibrations in pyrolytic graphite *Phys. Rev.* **128** 1120–3
- [42] Tan P H *et al* 2012 The shear mode of multilayer graphene *Nat. Mater.* **11** 294–300